Theoretical Comparison, Equivalent Transformation, and Conjunction Operations of Electromagnetic Induction Generator and Triboelectric Nanogenerator for Harvesting Mechanical Energy

*Chi Zhang, Wei Tang, Changbao Han, Fengru Fan, and Zhong Lin Wang**

Triboelectric nanogenerator (TENG) is a newly invented technology that is effective using conventional organic materials with functionalized surfaces for converting mechanical energy into electricity, which is light weight, cost-effective and easy scalable. Here, we present the first systematic analysis and comparison of EMIG and TENG from their working mechanisms, governing equations and output characteristics, aiming at establishing complementary applications of the two technologies for harvesting various mechanical energies. The equivalent transformation and conjunction operations of the two power sources for the external circuit are also explored, which provide appropriate evidences that the TENG can be considered as a current source with a large internal resistance, while the EMIG is equivalent to a voltage source with a small internal resistance. The theoretical comparison and experimental validations presented in this paper establish the basis of using the TENG as a new energy technology that could be parallel or possibly equivalently important as the EMIG for general power application at large-scale. It opens a field of organic nanogenerator for chemists and materials scientists who can be first time using conventional organic materials for converting mechanical energy into electricity at a high efficiency.

1. Introduction

With the rapid development of global economy in today's world, energy is one of the most important deciding factors that dictate the sustainable development of the human society. Various technologies have been invented and studied for harvesting energies from various sources, such as solar,[1] geothermal,[2] biomass,[3] wind[4] and wave power.[5] Among them, scavenging mechanical energy from the ambient environment are the most extensive emerging technologies, which have attracted great interests and are considered to be effective and promising approaches for solving the energy crisis due to the great abundance of mechanical energy existing in our living environment and industrial production.[6–11] Since the electromagnetic induction effect was discovered by Michael Faraday in 1831, the electromagnetic induction generator (EMIG) has been invented as one of the most important means for power generation in conjunction to turbine engine, including hydraulic, natural gas, nuclear, coal etc.[12–15] There has not been the second technology that is as important as the EMIG for power generation.

Recently, the invention of triboelectric nanogenerator (TENG) has provided an effective approach to generate electricity by harvesting mechanical energy with a different principle from the EMIG.[16–22] The working principle of the TENG is based on the coupling of the triboelectric effect and the electrostatic induction, which is about the applications of nanomaterials and nanotechnology for harvesting mechanical energy for powering micro/nanosystems. Moreover, the performance of the TENG has been improved by orders of magnitude ever since its invention in 2011,[23] and some theories of the TENG have been also explored and established.[24,25] Looking into the future, TENG can provide not only micro-scale energy for powering micro/nanosystems,[26] but also macro-scale energy for powering portable electronics[27] and household appliances,[28] which is likely to be a parallel or possibly equivalently important technology as the traditional EMIG for power generation.

Here in this work, we first gave systematic theoretical analysis and comparison of EMIG and TENG from their working mechanisms and governing equations. With the set parameters, we also compared and analyzed the output characteristics of both the generators in different circuit connections, and the equivalent transformation between the two is established as a power source, with the EMIG connected in series with the load resistance and the TENG in parallel connection with the

Dr. C. Zhang, Dr. W. Tang, Dr. C. B. Han,
Dr. F. R. Fan, Prof. Z. L. Wang
Beijing Institute of Nanoenergy and Nanosystems
Chinese Academy of Sciences
Beijing 100083, China
E-mail: zlwang@gatech.edu
Prof. Z. L. Wang
School of Material Science and Engineering
Georgia Institute of Technology
Atlanta, GA 30332, USA

DOI: 10.1002/adma.201400207

resistor. Finally, based on the two different electricity generating principles, a hybrid generator is designed and two hybrid operation modes in parallel and series are presented and characterized. This work not only presents the comparability and symmetry of the two groups of governing equations for EMIG and TENG, but also demonstrates that the TENG is equivalent to a current source with a large internal resistance, while the EMIG is equivalent to a voltage source with a small internal resistance. It has established the basis of the TENG as a new energy technology that could be equivalently important as the EMIG for general power application even at a large scale.

2. Theoretical Comparison of EMIG and TENG

The EMIG is based on the fundamental principle of the electromagnetic induction phenomenon, which is reviewed and schematically illustrated in **Figure 1**a. When a conductor stick with an external electric circuit moves across the magnetic induction lines, the induced electrodynamic potential is generated across the conductor stick:

$$E = B \cdot l \cdot v \tag{1}$$

where B is the magnetic flux density, l is the length of the conductor stick and v is the velocity of the conductor stick cutting the magnetic induction lines.

Unlike the EMIG, the TENG is based on the triboelectric effect and the electrostatic induction phenomenon to convert mechanical energy into electricity. The triboelectric effect is a contact-induced electrification in which a material becomes electrically charged after it is contacted with a different material through friction. The sign of the charges to be carried by a material depends on its relative polarity in comparison to the material to which it will contact. The electrostatic induction is a redistribution of electrical charges in an object caused by the influence of nearby charges in order to fully balance the electric field. In our previous works, there are mainly four basic operation modes of the TENG: vertical contact-separation mode,[29,30] in-plane sliding mode,[31,32] single-electrode mode[33,34] and freestanding-triboelectric-layer mode.[35] All of the modes have the same electricity generation process including producing electrostatic charges by triboelectrification, separating electrostatic charges by mechanical movement and generating induced current between two objects.

Compared to the other modes, the in-plane sliding-mode is more effective for static charges producing, and much easier for us to understand the electricity generation process, which is schematically illustrated in Figure 1b. In the original position, the surfaces of the top metal and the polymer interlayer fully overlap and intimately contact with each other. Because of the large difference in the ability to attract electrons, the triboelectrification will leave the top metal with net positive charges and the polymer surface with net negative charges with equal density as a result of transfer electrons from the metal to the polymer. When the top metal starts to slide outward, the in-plane charge separation is initiated due to the decrease in contact surface area. The separated charges will generate an electric field pointing from the right to the left almost parallel to the plates, inducing a higher potential at the top metal. This potential difference will drive a current flow from the top metal electrode to the bottom metal electrode in order to generate an electric potential drop that cancels the tribo-charge-induced potential. Because the vertical distance between the top metal and the tribo-charged polymeric surface is negligible compared to the lateral charge separation distance, the amount of the transferred charges between the top and bottom metals approximately equals to the amount of the separated charges at any sliding displacement if one neglects the edge effect. Thus, the current flow will continue with the continuation of the ongoing sliding process that keeps increasing the separated charges, which can be represented as:

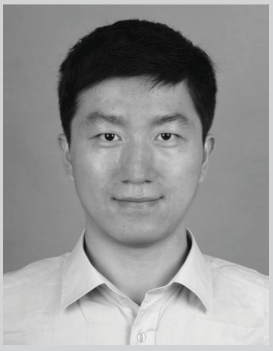

Dr. Chi Zhang is an associate professor in Beijing Institute of Nanoenergy and Nanosystems, Chinese Academy of Sciences. He received the B.S. degree from the Huazhong University of Science and Technology in 2004 and the Ph.D. degree from Tsinghua Univisity in 2009. After graduation, he worked in Tsinghua Univisity as a postdoc research fellow and NSK Ltd., Japan as a visiting scholar. His research interests are nanogenerator as active micro/nano sensors, self-powered MEMS/NEMS, flexible electronics and their applications in new energy technology, sensor networks and human-computer interaction.

Dr. Zhong Lin Wang is a Hightower Chair and Regents's Professor at Georgia Tech. He is also the Chief scientist and Director for the Beijing Institute of Nanoenergy and Nanosystems, Chinese Academy of Sciences. His discovery and breakthroughs in developing nanogenerators establish the principle and technological road map for harvesting mechanical energy from environment and biological systems for powering personal electronics. His research on self-powered nanosystems has inspired the worldwide effort in academia and industry for studying energy for micro-nano-systems, which is now a distinct disciplinary in energy research and future sensor networks. He coined and pioneered the field of piezotronics and piezo-phototronics by introducing piezoelectric potential gated charge transport process in fabricating new electronic and optoelectronic devices. This historical breakthrough by redesign CMOS transistor has important applications in smart MEMS/NEMS, nanorobotics, human-electronics interface and sensors.

Adv. Mater. **2014**,
DOI: 10.1002/adma.201400207

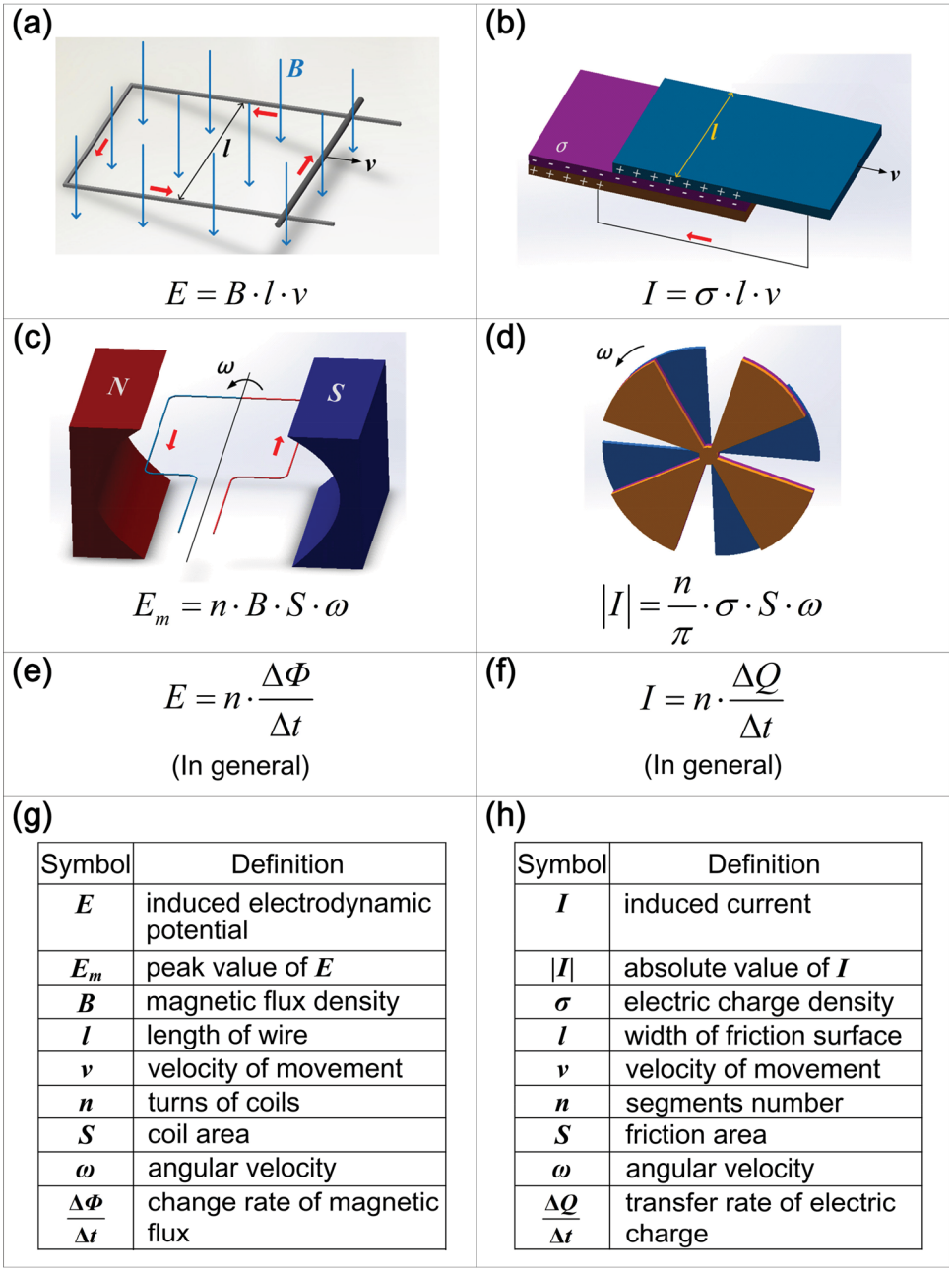

Symbol	Definition
E	induced electrodynamic potential
E_m	peak value of E
B	magnetic flux density
l	length of wire
v	velocity of movement
n	turns of coils
S	coil area
ω	angular velocity
$\frac{\Delta \Phi}{\Delta t}$	change rate of magnetic flux

Symbol	Definition
I	induced current
$\|I\|$	absolute value of I
σ	electric charge density
l	width of friction surface
v	velocity of movement
n	segments number
S	friction area
ω	angular velocity
$\frac{\Delta Q}{\Delta t}$	transfer rate of electric charge

Figure 1. Theoretical comparison of EMIG and TENG. (a,c,e,g) Schematic diagram, fundamental principles and governing equations of the electromagnetic induction generator (EMIG). (b,d,f,h) Schematic diagram, fundamental principles and governing equations of the triboelectric nanogenertor (TENG).

$$I = \frac{\sigma \cdot \Delta S}{\Delta t} = \sigma \cdot l \cdot v \tag{2}$$

where σ is the triboelectric charge density of the friction surface, l is the width of the friction surface perpendicular to the sliding direction and v is the sliding velocity of the top metal.

Compared with the two governing equations, we can find out the similar expressions and symmetric effects of them, which indicate that the TENG can generate the induced current as a current source while the EMIG can generate the induced voltage as a voltage source. The output current and voltage are both dependent on three physical variables, respectively. Firstly, the output current of the TENG depends on the triboelectric charge density, while the output voltage of the EMIG depends on the magnetic flux density, which are both determined by the intrinsic properties of the materials. Secondly, the output current of the TENG depends on the width of the friction surface perpendicular to the sliding direction, while the output voltage of the EMIG depends on the length of the conductor stick, which are both determined by the generator's size. Finally, the output current of the TENG depends on the sliding velocity of the top metal, while the output voltage of the EMIG depends

on the cutting velocity of the conductor stick, which are both determined by the input mechanical energy.

The schematic diagram of the rotating EMIG is reviewed and illustrated in Figure 1c. The rotating EMIG consists of a pair of magnets and a group of coils located in the magnetic field. When the coil rotates around the central axis, the magnetic flux through the coils is varying, which will generate an induced electrodynamic potential across the coils. The output voltage of the rotating EMIG is alternating as a sinusoidal wave, of which the peak value can be represented as:

$$E_m = n \cdot B \cdot S \cdot \omega \tag{3}$$

where n is the turns of coils, S is the area of a single turn of the coil and ω is the rotational angular velocity of the coil.

Figure 1d demonstrates a schematic diagram of the segmentally patterned disk-shaped rotating TENG,[36] in which a periodic overlapping and separation process of the two groups of sectors on the two concentric and closely contacted disks is achieved by relative rotation. The basic structure of the rotating TENG is composed of two disk-shaped components with several sectors each. The working principle is based on the triboelectrification and the relative-rotation induced cyclic in-plane charge separation between the top metal and polymer, which is the same as in the sliding-mode as shown in Figure 1a. Therefore, in the relative rotation, the electricity generation of the rotating TENG has a similar process as in the in-plane sliding-mode. When the top metal rotates in reference to the polymer, the corresponding two segments start to have a partially mismatched contact area, and the in-plane tribo-charges are thus separated in the direction almost parallel to the sliding direction, which will induce a higher potential on the top metal than the polymer, thus the electrons in the bottom metal attached to the polymer will be driven to flow to the top metal and keep flowing until the two disks are fully mismatch in the contacting segmented areas. As the top metal continues spinning, the polymer surface begins to contact another adjacent sector of the top metal, and the potential difference between two electrodes will drop with the decrease of the mismatch area. As a result, the electrons will flow back in the opposite direction from the top metal to the bottom metal attached to the polymer and keep flowing until the two disks reach a complete overlapping again. Thus, the entire process will result in an alternating current (AC) output as an approximate square wave with 50 percent duty cycle. The absolute value of the output current of the rotating TENG can be represented as:

$$|I| = \frac{\sigma \cdot \Delta S}{\Delta t} = \sigma \cdot \frac{n \cdot r^2 \cdot \Delta\theta}{2\Delta t} = \frac{n}{\pi} \cdot \sigma \cdot S \cdot \omega \tag{4}$$

where n is the segments number of the disk, S is the friction area of the disk (half area of the whole circle) and ω is the rotational angular velocity of the top metal.

The rotating EMIG and TENG both have an alternating output, which also have the similar and symmetric expressions in Equations (3) and (4). For the different output waves of sinsoidal and square in theory, the expressions have a difference of π in coefficients. The output current and voltage are both dependent on four physical variables, respectively. Firstly, the output current of the rotating TENG depends on the triboelectric charge density, while the output voltage of the rotating EMIG depends on the magnetic flux density. Secondly, the output current of the rotating TENG depends on the segments number of the disk, while the output voltage of the EMIG depends on the turns of coils, which are both determined by the generator's structure. Thirdly, the output current of the rotating TENG depends on the friction area of the disk, while the output voltage of the rotating EMIG depends on the coil area, which are both determined by the generator's size. Finally, the output current of the TENG depends on the rotational angular velocity of the top metal, while the output voltage of the EMIG depends on the rotational angular velocity of the coils, which are both determined by the input mechanical energy.

For the EMIG, the general governing equation is reviewed and represented as:

$$E = n \cdot \frac{\Delta\Phi}{\Delta t} \tag{5}$$

where n is the turns of coils, and $\Delta\Phi/\Delta t$ is the change rate of magnetic flux in each coil. For the TENG, no matter the operation mode is straight-line sliding, rotational sliding or other modes, the induced current is generated due to the transfer of electric charge between two objects. Therefore, the output current of the TENG can be described in a general governing equation as:

$$I = n \cdot \frac{\Delta Q}{\Delta t} \tag{6}$$

where n is the segments number which also represents the number of electric charge round-trips between two objects in a unit time, and $\Delta Q/\Delta t$ is the transfer rate of electric charge in each segment. Compared with the two general governing equations, we can see that the TENG supplies induced current due to the transferring electric charge, while the EMIG supplies induced voltage due to the changing magnetic flux.

The fundamental principles, rotational structures, governing equations and significances of symbols of the EMIG and TENG are illustrated and described all together in Figure 1 for comparison. The results of the analysis and comparison in above indicate that the TENG has a comparative and symmetric relationship with the traditional EMIG in theory, which can be considered as a current source while the EMIG is considered as a voltage source.

3. Output Characteristics of EMIG and TENG

Besides the theoretical comparison, the output characteristics of the rotating EMIG and TENG are also compared with two sets of parameters as detailed in **Table 1**. The rotating TENG is designed with four sectors structure and the empirical triboelectric charge density of 70 μC/m^2, while the rotating EMIG is designed with twelve turns of a coil and the magnetic flux density of 0.05 T. The friction area of the TENG is 12.4 cm^2 and the coil area of the EMIG is 25.3 cm^2. The disk surface of the TENG is two times of the friction area that is approximately

Adv. Mater. 2014,
DOI: 10.1002/adma.201400207

Table 1. Parameters design of EMIG and TENG.

EMIG		TENG	
Turns of coils	$n_1 = 12$	Segments number	$n_2 = 4$
Magnetic flux density	B = 0.05 T	Triboelectric charge density	$\sigma = 70\ \mu C/m^2$
Coil area	$S_1 = 25.3\ cm^2$	Friction area	$S_2 = 12.4\ cm^2$
Angular velocity	$\omega = 20\pi$ rad/s	Angular velocity	$\omega = 20\pi$ rad/s
Induced electrodynamic potential	$E_m = 95.3$ mV	Induced current	I = 6.94 μA

the coil area of the EMIG. Both of them have the same angular velocity of 20π rad/s. According to Equations (3) and (4), the induced peak voltage of the EMIG is 95.3 mV and the induced current of the TENG is 6.94 μA in theoretical calculation.

The electric brushes are used for the rotating EMIG to convert the AC output into the direct current (DC) output and the output characteristics of the DC-EMIG are systematically studied at different external resistive load. Figure S1 shows the real-time output voltage of the EMIG applied on the resistance of 10 kΩ and **Figure 2**a shows both the effective values of output current and voltage under different load from 1 Ω to 10 kΩ. The output current decreases with the increasing resistance while the output voltage shows the reverse trend, but both the current and voltage tend to saturate when the resistance is considerably large. The measured open circuit output voltage is 67.6 mV, which accords well with the theoretical peak value of the sinusoidal induced voltage. The output power is also plotted as a function of the external resistance in Figure 2b. The maximum output power of 102.6 μW is received when the external resistance is 12.3 Ω. The experimental results indicate that the matching impedance of the EMIG is 12.3 Ω for receiving the maximum output power due to the EMIG has a small internal resistance owing to the conductive coils. When the external resistive load is considerably larger than the internal resistance, the EMIG is equivalent to be considered as a voltage source.

The output of the rotating TENG is also converted into the DC output as a constant current wave by the electric brushes[37] and systematically characterized at different external resistive load. Figure S2 shows the real-time output current of the TENG applied on the resistance of 10 Ω and **Figure 3**a shows the resistance dependence of both output current and voltage, from 10 Ω to 500 MΩ. As with the EMIG, the output current decreases with the increasing resistance while the output voltage shows the reverse trend, but both the current and voltage curves are smooth when the resistance is small. The measured short-circuit output current is 6.96 μA, which accords with the theoretical value of the induced current well. Figure 3b shows the output power as a function of external resistance. The output power increases at a lower resistance region and then decreases at a higher resistance region. The maximum output power of 140.4μW is received when the external resistance is 13.8 MΩ. Therefore, the TENG can be equivalent to be considered as a current source with a large internal resistance when the external resistive load is considerably smaller than the internal resistance.

The output power of the rotating DC-EMIG and DC-TENG are compared in **Figure 4**a. The matching impedances for

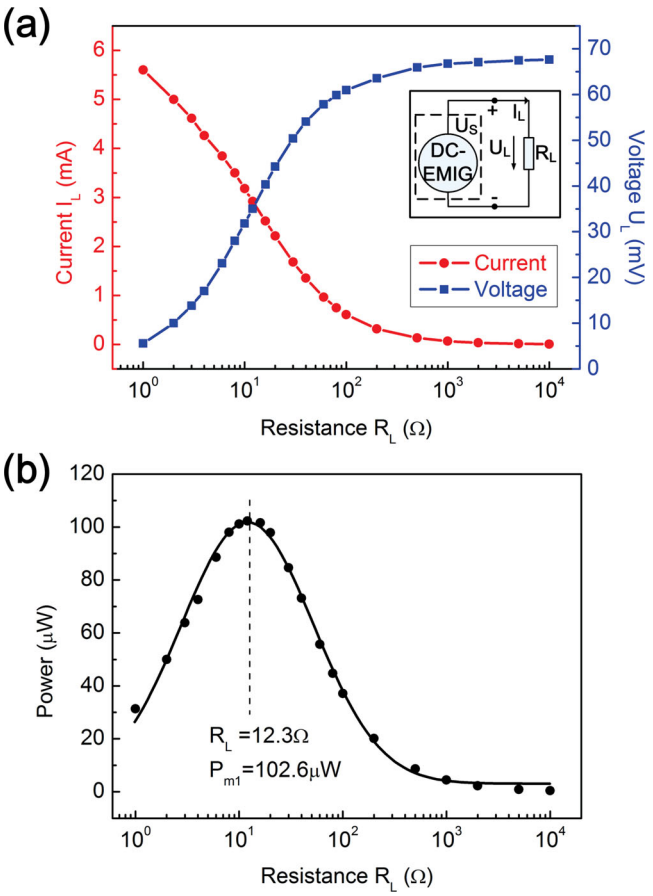

Figure 2. Output characteristics with different external resistive load of the rotating DC-EMIG. (a) The relationship between the output voltage/current and the resistance of the external load. The inset is the circuit diagram of the rotating DC-EMIG with external resistive load. (b) The relationship between the output power and the resistance of the external load. The maximum power of 102.6 μW is received when the external resistance is 12.3 Ω.

receiving the maximum output powers from them are gigantically different in magnitude and the measured maximum output power of the rotating DC-TENG is slightly larger than the DC-EMIG. The output power per unit volume and mass of the two generators are also measured and plotted in Figure 4b and 4c. Due to the EMIG has two thick and heavy magnets but the TENG has two supported organic glass plates with smaller volume and lower weight, the maximum power per unit volume is 0.36 W/m^3 for the EMIG and 3.11 W/m^3 for the TENG, as well as the maximum power per unit mass is 0.25 mW/kg for the EMIG and 2.63 mW/kg for the TENG. Obviously, considering the size and weight, the TENG has significantly larger output power and more advantages over the EMIG.

The measured characteristics including the electric output, internal resistance, maximum power, volume and mass of the EMIG and TENG are summarized all together in **Table 2** for comparison, which quantitatively supports the theoretical comparison and well validated that the TENG is a distinct but likely to be a parallelly important technology as the traditional EMIG for power generation.

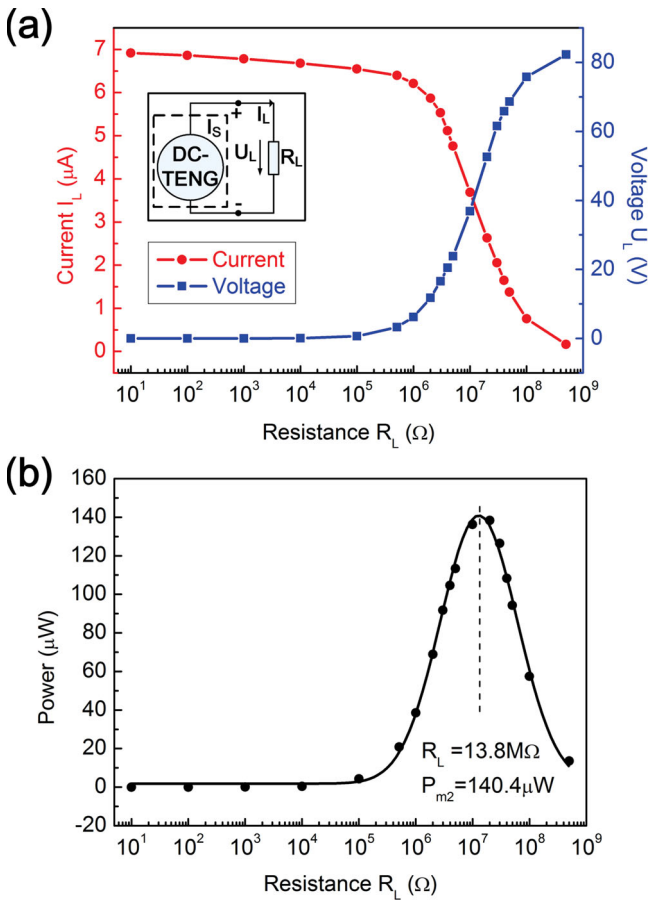

Figure 3. Output characteristics with different external resistive load of the rotating DC-TENG. (a) The relationship between the output voltage/current and the resistance of the external load. The inset is the circuit diagram of the rotating DC-TENG with external resistive load. (b) The relationship between the output power and the resistance of the external load. The maximum power of 140.4 μW is received when the external resistance is 13.8 MΩ.

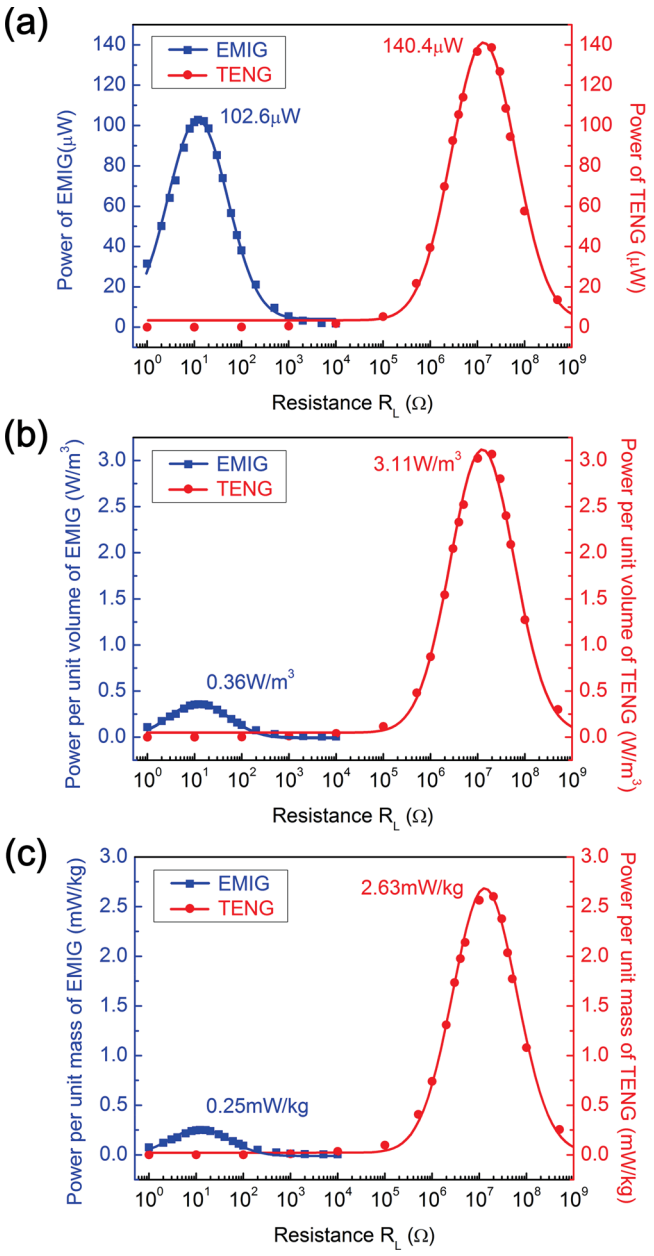

Figure 4. Output power comparison of the rotating DC-EMIG and DC-TENG. (a) The output power of the rotating DC-EMIG and DC-TENG with different external resistive load. (b) The output power per unit volume of the rotating DC-EMIG and DC-TENG with different external resistive load. The maximum power per unit volume is 0.36 W/m^3 for the EMIG and 3.11 W/m^3 for the TENG. (c) The output power per unit mass of the rotating DC-EMIG and DC-TENG with different external resistive load. The maximum power per unit mass is 0.25 mW/kg for the EMIG and 2.63 mW/kg for the TENG.

4. Equivalent Transformation between EMIG and TENG

An ideal voltage source has zero internal resistance and the output voltage is independent of the external load, while an ideal current source has infinite internal resistance and the output current is independent of the external load. In the circuit, if an ideal voltage source is connected with an ideal current source in parallel, the output voltage and current on the external load is dictated by the voltage source. On the contrary, if an ideal voltage source is connected with an ideal current source in series, the output voltage and current on the external load is dictated by the current source.

The output characteristics of the rotating DC-EMIG and DC-TENG in parallel and series connection are measured and analyzed. **Figure 5**a shows the output current and voltage by varying the load resistance, from 1 Ω to 10 kΩ. The output power is also plotted as a function of external resistance in Figure 5b. The measured saturation value of the effective output voltage is 67.5 mV and the maximum power 103.1 μW is received when the external resistance is 12.3 Ω. The measured curve and values are nearly identical as those for the rotating DC-EMIG as shown in Figure 2, indicating that the parallel connection of the EMIG and TENG is nearly equivalent to the EMIG for the external load. Likewise, **Figure 6**a shows the resistance dependence of the output

Adv. Mater. **2014**,
DOI: 10.1002/adma.201400207

Table 2. Characteristics comparison of EMIG and TENG.

EMIG		TENG	
Open-circuit voltage	$U_S = 67.6$ mV	Short-circuit current	$I_S = 6.96$ μA
Internal resistance	$R_{01} = 12.3$ Ω	Internal resistance	$R_{02} = 13.8$ MΩ
Maximum power	$P_{m1} = 102.6$ μW	Maximum power	$P_{m2} = 140.4$ μW
Volume	$V_1 = 288$ cm^3	Volume	$V_2 = 45.2$ cm^3
Mass	$M_1 = 412$ g	Mass	$M_2 = 53.3$ g
Maximum power per unit volume	$P_{V1} = 0.36$ W/m^3	Maximum power per unit volume	$P_{V2} = 3.11$ W/m^3
Maximum power per unit mass	$P_{M1} = 0.25$ mW/kg	Maximum power per unit mass	$P_{M2} = 2.63$ mW/kg

current and voltage when the two are connected in series. The output power is plotted as a function of external resistance in Figure 6b. The measured short-circuit output current is 6.94 μA and the maximum power 140.4 μW is received when the external resistance is 13.8 MΩ. The measured curve and values are almost the same as those for the rotating DC-TENG as shown in Figure 3, which indicate that a serial connection of the EMIG and TENG is nearly equivalent to the TENG for the external load. The experimental results further validate the characteristics of the TENG as a current source while the EMIG as a voltage source.

A practical voltage source can be represented as an ideal voltage source in series connection with an internal resistance, while a current source can be represented as an ideal current source in parallel connection with an internal resistance. For the external load, an practical power source is equivalent to either a voltage source or a current source, and the voltage and current sources can be equivalently transformed with each other.

The rotating DC-EMIG is in series connection with a resistance R_S as a power source for the external load, which is displayed in the inset of **Figure 7**a, while the rotating DC-TENG is in parallel connection with the resistance R_S of the same

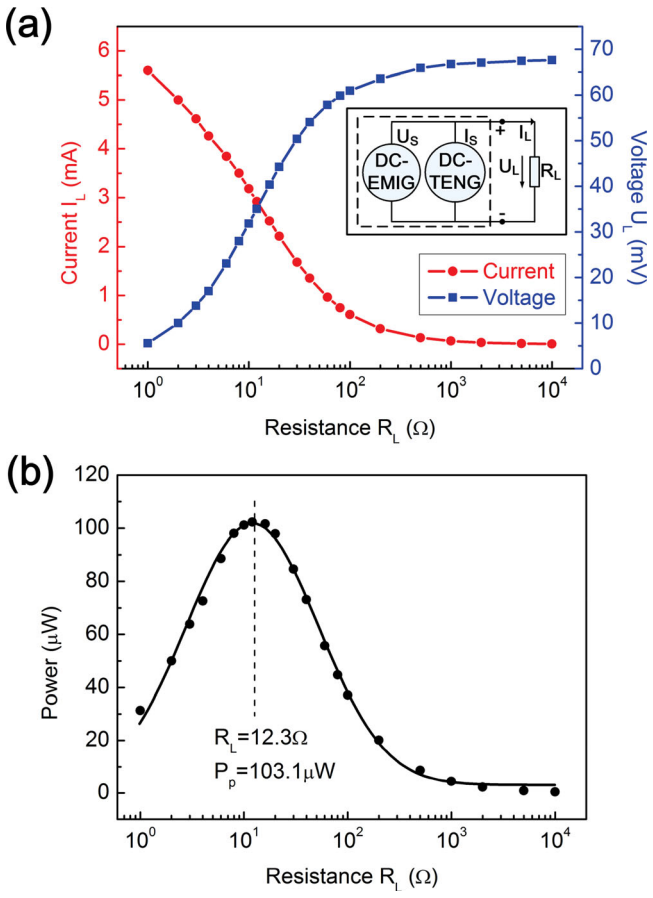

Figure 5. Output characteristics with different external resistive load of the rotating DC-EMIG and DC-TENG in parallel connection. (a) The relationship between the output voltage/current and the resistance of the external load. The inset is the circuit diagram of the rotating DC-EMIG and DC-TENG in parallel connection with external resistive load. (b) The relationship between the output power and the resistance of the external load. The maximum power of 103.1 μW is received when the external resistance is 12.3 Ω.

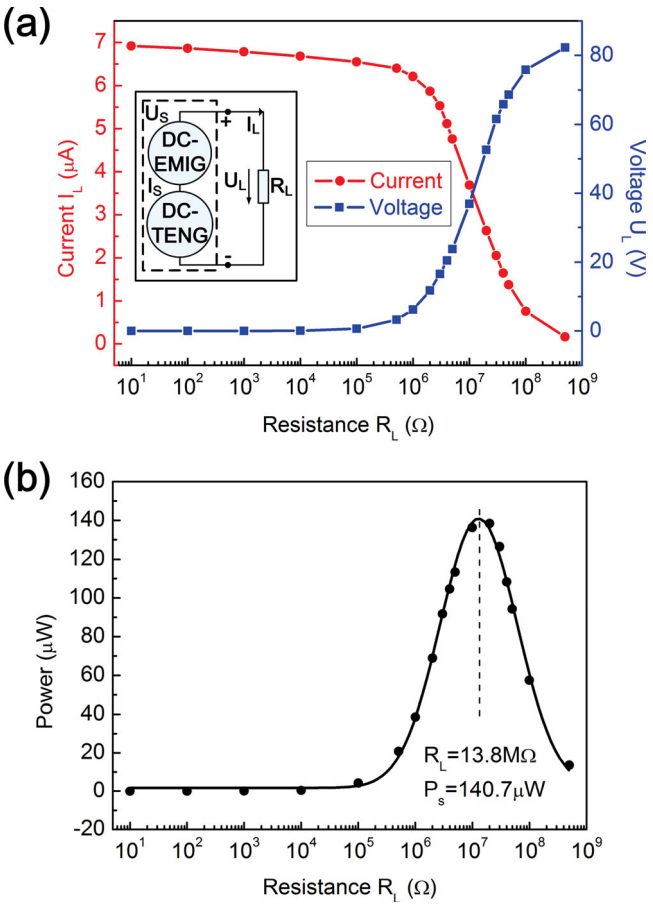

Figure 6. Output characteristics with different external resistive load of the rotating DC-EMIG and DC-TENG in serial connection. (a) The relationship between the output voltage/current and the resistance of the external load. The inset is the circuit diagram of the rotating DC-EMIG and DC-TENG in serial connection with external resistive load. (b) The relationship between the output power and the resistance of the external load. The maximum power of 140.7 μW is received when the external resistance is 13.8 MΩ.

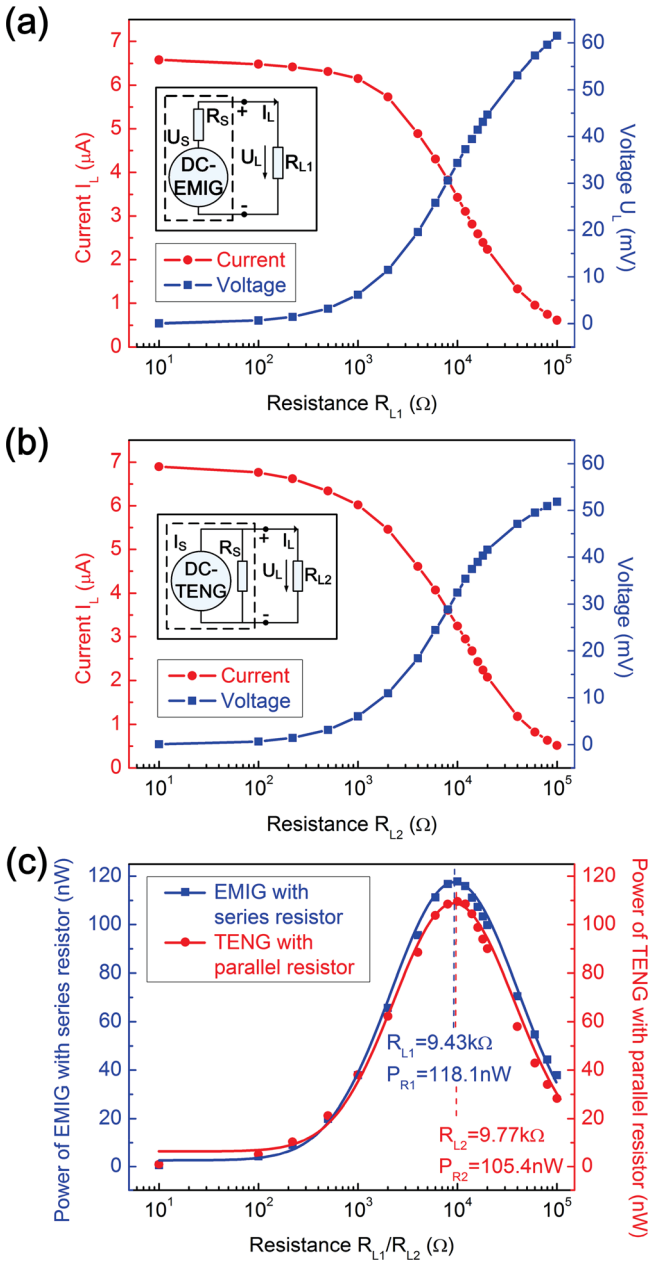

Figure 7. Equivalent transformation between the rotating DC-EMIG and DC-TENG with the resistor R_S. (a) The relationship between the output voltage/current and the resistance of the external load for the rotating DC-EMIG connected in series with the resistor R_S. The inset is the circuit diagram. (b) The relationship between the output voltage/current and the resistance of the external load for the rotating TENG in parallel connection with the resistor R_S. The inset is the circuit diagram. (c) The relationship between the output power and the resistance of the external load. The maximum power of 118.1 nW is received when the external resistance is 9.43 kΩ for the rotating DC-EMIG connected in series with the resistor R_S, while the maximum power of 105.4 nW is received when the external resistance is 9.77 kΩ for the rotating DC-TENG in parallel connection with the resistor R_S.

value as another power source for the external load, which is displayed in the inset of Figure 7b. The resistance value of R_S is determined by the equivalent condition as:

$$R_S = \frac{U_S}{I_S} \tag{7}$$

where U_S is the measured open-circuit voltage (67.6 mV), I_S is the measured short-circuit current (6.96 μA) and the resistance value of R_S is 9.71 kΩ in this case. If the DC-EMIG is considered as an ideal voltage source and the DC-TENG is considered as an ideal current source in the circuit, according to Kirchhoff's law, when the external resistive load R_{L1} is equal to R_S, the maximum output power of the power source can be expressed as:

$$P_R = \frac{1}{4} U_S \cdot I_S \tag{8}$$

The theoretical value of the maximum output power is 117.6 nW in this case. By the same token, when the external resistive load R_{L2} is equal to R_S, the maximum output power of the other power source can be expressed by Equation (8) and the theoretical value is 117.6 nW as well.

The output current and voltage curves of the two power sources are shown in Figure 7a and 7b, respectively, depended on different external resistance from 10 Ω to 100 kΩ. The output power curves are plotted as two load resistances in Figure 7c, which nearly overlap with each other. The maximum power of 118.1 nW is received when the external resistance is 9.43 kΩ for the power source using DC-EMIG in series connection with the resistance R_S. A maximum power of 105.4 nW is received when the external resistance is 9.77 kΩ for the power source using DC-TENG connected in parallel with the resistance R_S. The both matching impedances for receiving the maximum output powers of the two power sources are very close to the designed value of 9.71 kΩand both the maximum output powers are very close to the theoretical value of 117.6 nW as well.

The experimental results validate the equivalent transformation between the two power sources for the external circuit, with the EMIG connected in series with the load resistance and the TENG in parallel connection with the resistor. The equivalent transformation has established a correlation between the EMIG and TENG for practical applications.

5. Conjunction Operations of EMIG and TENG

Based on the two different electricity generating principles, a hybrid generator of the rotating DC-EMIG and DC-TENG is designed, which is schematically and practically illustrated in **Figure 8**a. The two generators have a common rotational axis and the input mechanical energy can simultaneously drive both generators under the same angular velocity. The output characteristics of the hybrid generator are measured and analyzed in different conjunction operation modes of the EMIG and TENG.

On the one hand, the DC-EMIG with the serial resistor R_S of 9.71 kΩ and the DC-TENG with the parallel resistor R_S of the same value are connected in the parallel mode as a power source for the external circuit, which is displayed in the inset of Figure 8b. On the other hand, the DC-EMIG with the

Adv. Mater. **2014**,
DOI: 10.1002/adma.201400207

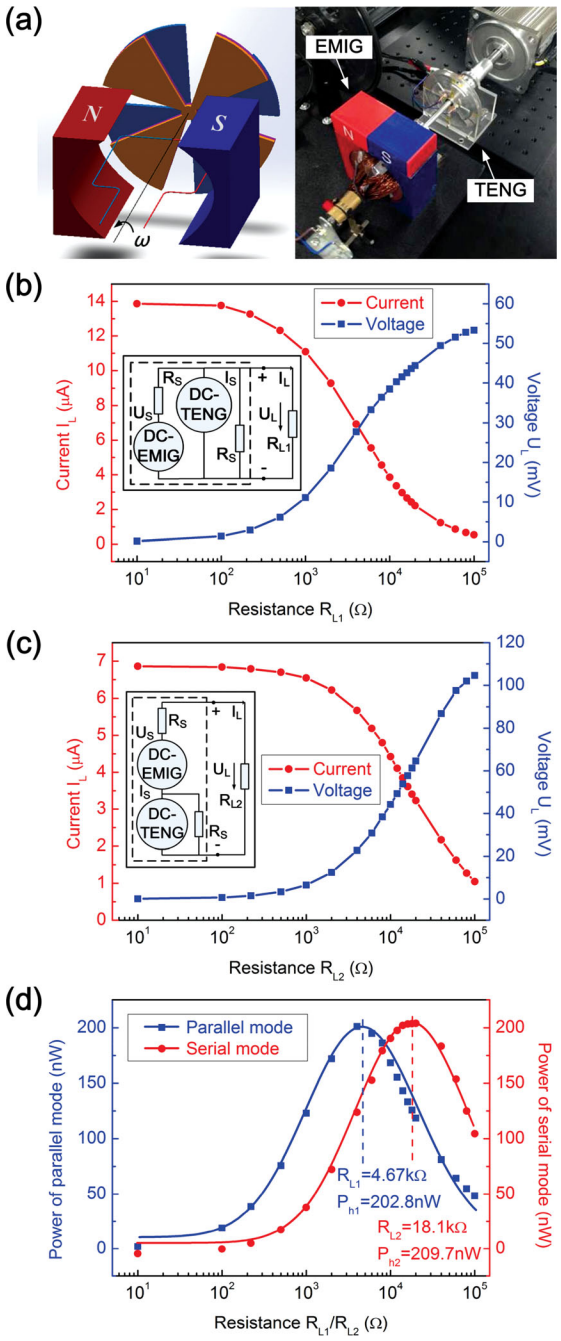

Figure 8. Conjunction operations of the rotating DC-EMIG and DC-TENG. (a) The schematic diagram and photo of the hybrid generator. (b) The relationship between the output voltage/current and the resistance of the external load in the parallel mode. The inset is the circuit diagram of the rotating DC-EMIG with the serial resistor R_S and the rotating DC-TENG with the parallel resistor R_S in the parallel mode. (c) The relationship between the output voltage/current and the resistance of the external load in the serial mode. The inset is the circuit diagram of the rotating DC-EMIG with the serial resistor R_S and the rotating DC-TENG with the parallel resistor R_S in the serial mode. (d) The relationship between the output power and the resistance of the external load in both modes. The maximum power 202.8 nW is received when the external resistance is 4.67 kΩ in the parallel mode, while the maximum power of 209.7 nW is received when the external resistance is 18.1 kΩ in the serial mode.

serial resistor R_S of 9.71 kΩ and the DC-TENG with the parallel resistor R_S of the same value are connected in the serial mode as another power source for the external circuit, which is displayed in the inset of Figure 8c. According to Kirchhoff's law, when the external resistive load R_{L1} is equal to half of the resistance R_S, the maximum output power of the power source can be expressed as:

$$P_h = \frac{1}{2} U_S \cdot I_S \tag{9}$$

The theoretical value of the maximum output power is 235.2 nW in this case. By the same token, when the external resistive load R_{L2} is equal to two times of the resistance R_S, the maximum output power of the other power source can be expressed by Equation (9) and the theoretical value is 235.2 nW as well.

Figure 8b and 8c show the resistance dependence of output current and voltage curves of the both power sources, respectively, from 10 Ω to 100 kΩ. The output powers are also plotted as function of external resistance in Figure 8d. The maximum power of 202.8 nW is received when the external resistance is 4.67 kΩ for the two power sources in parallel connection, while the maximum power of 209.7 nW is received when the external resistance is 18.1 kΩ for the two power sources in serial connection.

The experimental results show that the maximum powers in the two connection modes are both close to the theoretical value of 235.2 nW and approximately two times of the two power sources in the insets of Figure 7a and 7b, respectively. The output power is superposed by each part of the power source in either parallel or serial mode. The matching impedance for receiving the maximum output power in the parallel mode is approximately half of the resistance R_S; the matching impedance for receiving the maximum output power in the serial mode is approximately two times of the resistance R_S. The output characteristics of the two conjunction operation modes follows well with the theoretical analysis based on Kirchhoff's law if the EMIG is considered as an ideal voltage source and the TENG is considered as an ideal current source.

6. Materials Aspects for High-Performance TENG

Triboelectrification effect is a universally known phenomenon and any materials can have this effect, from metal, to polymer, to silk and to wood, almost everything. The materials choices for TENG are huge, much broader than materials for any other energy harvesting technologies. The ability of a material for gaining/losing electron depends on its polarity. Although it has not been quantitatively documented using a specific number, there is a tendency of materials for lossing/retaining electrons, so call the triboelectric series (**Table 3**).[38] Choosing two materials that are largely separated in the triboelectric series will give the higher performnace TENG output (**Figure 9**a).

The morphologies of the materials surfaces can be modified by physical techniques with the creation of pyramids-,

Table 3. Triboelectric series for some commonly materials following a tendency of easy losing electrons (positive) to gaining electrons (negative) [from[38]].

Positive	Polyformaldehyde 1.3–1.4	(continued)
	Etylcellulose	Polyester (Dacron)
	Polyamide 11	Polyisobutylene
	Polyamide 6–6	Polyuretane flexible sponge
	Melanime formol	Polyethylene Terephthalate
	Wool, knitted	Polyvinyl butyral
	Silk, woven	Polychlorobutadiene
	Aluminum	Natural rubber
	paper	Polyacrilonitrile
	Cotton, woven	Acrylonitrile-vinyl chloride
	Steel	Polybisphenol carbonate
	Wood	Polychloroether
	Hard rubber	Polyvinylidine chloride (Saran)
	Nickel, copper	Polystyrene
	Sulfur	Polyethylene
	Brass, silver	Polypropylene
	Acetate, Rayon	Polyimide (Kapton)
	Polymethyl methacrylate (Lucite)	Polyvinyl Chloride (PVC)
	Polyvinyl alcohol	Polydimethylsiloxane (PDMS)
	(continued)	Polytetrafluoroethylene (Teflon)
		Negative

square- or hemisphere-based micro- or nano-patterns, which are effective for enhancing the contact area and possibly the triboelectrification (Figure 9b). The surfaces of the materials can be functionalized chemically using various molecules, nanotubes, nanowires or nanoparticles, in order to enhance the triboelectrification effect.[30] Surface functionalization can largely change the surface contact area, surface charge transfer density and the surface friction coefficient. The materials can be made of composites, such embedding nanoparticles, nanowires, nanotubes in polymer matrix.[39] This not only changes the surface electrification, but also the permittivity of the materials so that they can be effective for electrostatic induction. Therefore, there are numerous ways for enhancing the performance of the TENG from the materials point of view. This gives an excellent opportunity for chemists and materials scientists to use the advanced materials they have developed for improving the performance of the TENG, which is probably the first application of organic materials for converting mechanical energy. Lastly and importantly, it will be an outstanding research for improving the durability and stability of the TENG over millions/billions of cycles of service while preserving its high performance.

7. Conclusion

In summary, we present the analysis and comparison in details of the theoretical models, working mechanisms and governing equations of the EMIG and TENG for harvesting mechanical energy, which has a comparative and symmetric relationship with each other. The TENG is a current source with a large internal resistance, and the EMIG is equivalent to a voltage source with a small internal resistance. Moreover, the equivalent transformation between the two power sources for driving an external circuit is validated, with the EMIG connected in series with a resistor and the TENG in parallel connection with a resistor. Finally, a hybrid generator based on the two different electricity generating principles is presented and characterized in different circuit connections, which are in good agreement with the theoretical analysis. Our theoretical comparison and experimental validations is a milestone for in-depth analysis and comparison between the TENG and the traditional EMIG, and establishes the basis of using the TENG as a new energy technology that could be equivalently important as the EMIG for general power application.

Lastly, we present the projection of how advanced materials will largely enhance the performance of the TENG. TENG can be made using conventional polymer films and metal films, and it can be fully optically transparent, largely flexible/stretchable and shape adaptable. The materials can from thin films, nanostructured composites, surface functionalized groups and more. TENG opens a field of organic nanogenerator for chemists and materials scientists who can be first time using conventional organic materials for converting mechanical energy into electricity at a high efficiency.

Adv. Mater. **2014**,
DOI: 10.1002/adma.201400207

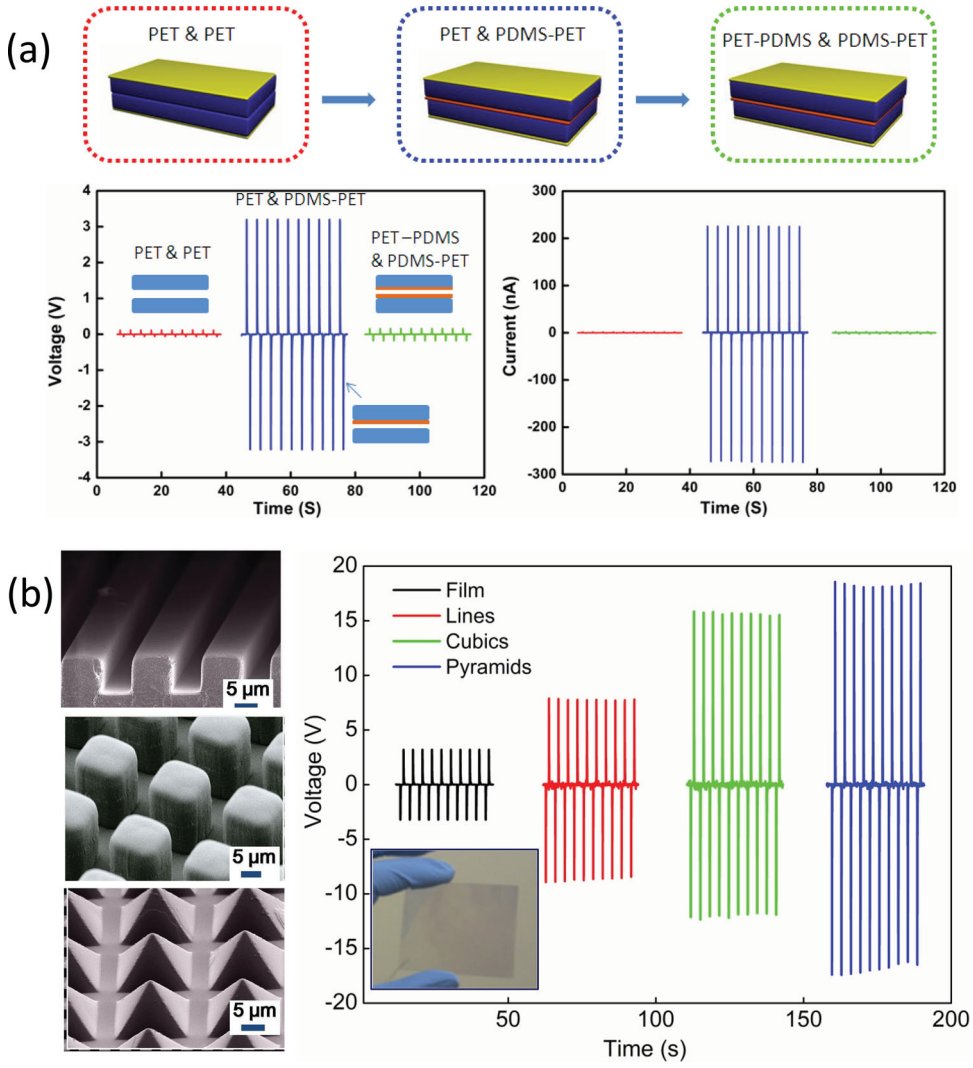

Figure 9. Choices of materials and surface characteristics for high-performance organic TENG. (a) Performance characterization of TENGs made using PET and PDMF at different sequential layers. The output voltages of FTNGs made of PET&PET and PET-PDMS&PDMS-PET are far lower than that of PET&PDMS-PET. It clearly indicates that we should use materials with distinct triboelectric characteristics to get high output. (b) SEM images of the microstructured PDMS films: rectangular line, square cubes, and square pyramids. Performance characterization of the TENS made using different patterned a flat PET film but PDMS films that are flat, with rectangular line, square cube, or square pyramid. The inset is a transparent, flexible TENG, reprouced with permission from references[16,17]. Copyright 2012, Elsevier and Copyright 2012, American Chemical Society.

Supporting Information

Supporting Information is available from the Wiley Online Library or from the author.

Acknowledgements

Thanks for the support from the "thousands talents" program for pioneer researcher and his innovation team, China; and the Beijing Municipal Science & Technology Commission (Z131100006013004, Z131100006013005).

Received: January 14, 2014
Revised: February 12, 2014
Published online:

[1] D. Wöhrle, D. Meissner, *Adv. Mater.* **1991**, *3*, 129.
[2] J. W. Lund, D. H. Freeston, *Geothermics* **2000**, *30*, 29.
[3] P. McKendry, *Bioresource Technol.* **2002**, *83*, 37.
[4] R. Doherty, M. O'Malley, *IEEE T. Power Syst.* **2005**, *20*, 587.
[5] M. Leijon, H. Bernhoff, O. Agren, J. Isberg, J. Sundberg, M. Berg, K. E. Karlsson, A. Wolfbrandt, *IEEE T. Energy Conver.* **2005**, *20*, 219.
[6] B. Z. Tian, X. L. Zheng, T. J. Kempa, Y. Fang, N. F. Yu, G. H. Yu, J. L. Huang, C. M. Lieber, *Nature* **2007**, *449*, 885.
[7] M. S. Dresselhaus, G. Chen, M. Y. Tang, R. G. Yang, H. Lee, D. Z. Wang, Z. F. Ren, J. P. Fleurial, P. Gogna, *Adv. Mater.* **2007**, *19*, 1043.
[8] B. Oregan, M. Gratzel, *Nature* **1991**, *353*, 737.
[9] E. P. Murray, T. Tsai, S. A. Barnett, *Nature* **1999**, *400*, 649.
[10] K. I. Park, S. Xu, Y. Liu, G. T. Hwang, S. J. L. Kang, Z. L. Wang, K. J. Lee, *Nano Lett.* **2010**, *10*, 4939.
[11] S. Xu, Y. Qin, C. Xu, Y. Wei, R. Yang, Z. L. Wang, *Nat. Nanotechnol.* **2010**, *5*, 366.

[12] C. B. Williams, C. Shearwood, M. A. Harradine, P. H. Mellor, T. S. Birch, R. B. Yates, *IEE Proc. Circuits Devices Syst.* **2001**, *148*, 337.
[13] P. D. Mitcheson, T. C. Green, E. M. Yeatman, A. S. Holmes, *J. Microelectromech S.* **2004**, *13*, 429.
[14] C. R. Saha, T. O'Donnell, H. Loder, S. Beeby, J. Tudor, *IEEE T. Magn.* **2006**, *42*, 3509.
[15] D. P. Arnold, *IEEE T. Magn.* **2007**, *43*, 3940.
[16] F. R. Fan, Z. Q. Tian, Z. L. Wang, *Nano Energy* **2012**, *1*, 328.
[17] F. R. Fan, L. Lin, G. Zhu, W. Z. Wu, R. Zhang, Z. L. Wang, *Nano Lett.* **2012**, *12*, 3109.
[18] G. Zhu, C. F. Pan, W. X. Guo, C. Y. Chen, Y. S. Zhou, R. M. Yu, Z. L. Wang, *NanoLett.* **2012**, *12*, 4960.
[19] X. S. Zhang, M. D. Han, R. X. Wang, F. Y. Zhu, Z. H. Li, W. Wang, H. X. Zhang, *Nano Lett.* **2013**, *13*, 1168.
[20] J. W. Zhong, Q. Z. Zhong, F. R. Fan, Y. Zhang, S. H. Wang, B. Hu, Z. L. Wang, J. Zhou, *Nano Energy* **2012**, *2*, 491.
[21] T. C. Hou, Y. Yang, H. L. Zhang, J. Chen, L. J. Chen, Z. L. Wang, *Nano Energy* **2013**, *2*, 856.
[22] P. Bai, G. Zhu, Z. H. Lin, Q. S. Jing, J. Chen, G. Zhang, J. S. Ma, Z. L. Wang, *ACS Nano* **2013**, *7*, 3713.
[23] Z. L. Wang, *ACS Nano* **2013**, *7*, 9533.
[24] S. M. Niu, S. H. Wang, L. Lin, Y. Liu, Y. S. Zhou, Y. F. Hu, Z. L. Wang, *Energ. Environ. Sci.* **2013**, *6*, 3576.
[25] S. M. Niu, Y. Liu, S. H. Wang, L. Lin, Y. S. Zhou, Y. F. Hu, Z. L. Wang, *Adv. Mater.* **2013**, *25*, 6184.
[26] Z. L. Wang, W. Z. Wu, *Angew. Chem., Int. Ed.* **2012**, *51*, 11700.
[27] Z. L. Wang, G. Zhu, Y. Yang, S. H. Wang, C. F. Pan, *Mater. Today* **2013**, *15*, 532.
[28] G. Zhu, Y. S. Zhou, P. Bai, X. S. Meng, Q. S. Jing, J. Chen, Z. L. Wang, *Adv. Mater.in press* **2014**.
[29] S. H. Wang, L. Lin, Z. L. Wang, *NanoLett.* **2012**, *12*, 6339.
[30] G. Zhu, Z. H. Lin, Q. S. Jing, P. Bai, C. F. Pan, Y. Yang, Y. S. Zhou, Z. L. Wang, *Nano Lett.* **2013**, *13*, 847.
[31] S. H. Wang, L. Lin, Y. N. Xie, Q. S. Jing, S. M. Niu, Z. L. Wang, *Nano Lett.* **2013**, *13*, 2226.
[32] G. Zhu, J. Chen, Y. Liu, P. Bai, Y. S. Zhou, Q. S. Jing, C. F. Pan, Z. L. Wang, *Nano Lett.* **2013**, *13*, 2282.
[33] Y. Yang, Y. S. Zhou, H. L. Zhang, Y. Liu, S. Lee, Z. L. Wang, *Adv. Mater.* **2013**, *25*, 6594.
[34] Y. Yang, H. L. Zhang, J. Chen, Q. S. Jing, Y. S. Zhou, X. N. Wen, Z. L. Wang, *ACS Nano* **2013**, *7*, 7342.
[35] S. H. Wang, Y. N. Xie, S. M. Niu, L. Lin, Z. L. Wang, *Adv. Mater.* **2013**, DOI: 10.1002/adma.201305303.
[36] L. Lin, S. H. Wang, Y. N. Xie, Q. S. Jing, S. M. Niu, Y. F. Hu, Z. L. Wang, *Nano Lett.* **2013**, *13*, 2916.
[37] C. Zhang, T. Zhou, W. Tang, C. B. Han, L. M. Zhang, Z. L. Wang, *Adv. Energy Mater.* **2014**, DOI: 10.1002/aenm.201301798.
[38] D. K. Davies, *J Phys D Appl Phys* **1969**, *2*, 1533.
[39] Y. Yang, H. Zhang, S. Lee, T.-C. Hou, Z. L. Wang, *Energy & Environemntal Sci.* **2013**, *6*, 1744.

Adv. Mater. **2014**,
DOI: 10.1002/adma.201400207